

VOYAGER MEASUREMENTS OF THE MASS COMPOSITION OF COSMIC-RAY Ca THROUGH Fe NUCLEI

A. LUKASIAK AND F. B. McDONALD

Institute for Physical Science and Technology, University of Maryland, College Park, MD 20742-2431;
al36@umail.umd.edu, fm27@umail.umd.edu

AND

W. R. WEBBER

Astronomy Department, New Mexico State University, Las Cruces, NM 88003; wwebber@nmsu.edu

Received 1996 December 13; accepted 1997 May 22

ABSTRACT

We present measurements of the charge and isotopic composition of cosmic-ray Ca through Fe nuclei made on the *Voyager* spacecraft. We have analyzed 18 years of data in the energy range 100–300 MeV nucleon⁻¹ collected by the High Energy Telescope of the cosmic-ray subsystem experiment on the *Voyager 1* and 2 spacecraft. The average solar modulation level for this measurement is 480 MV. These data have several times the statistical accuracy and have mass resolution comparable to the best previously published measurements covering this charge range from the *ISEE* cosmic-ray experiment. Many of the isotopes of these charges are dominated by secondary production from cosmic rays traversing the interstellar medium, and for these isotopes our measured isotopic fractions are generally consistent to within 10%, with the exception of certain K-capture isotopes, with those calculated for secondary production using the latest propagation codes and cross sections. For five isotopes, ⁴⁰Ca, ⁵²Cr, ⁵⁵Mn, ⁵⁴Fe, and ⁵⁸Fe, we can determine the cosmic-ray source composition to an improved accuracy over previous values. None of these isotopes show any significant differences with respect to the solar composition. This result, taken with other recent *Voyager* measurements of the isotopic composition of charge $Z = 6$ –16 nuclei as well as Co and Ni nuclei, now provide the source composition of ~ 20 individual cosmic-ray isotopes with Z between 6 and 28 measured by the same instrument under the same conditions. This source composition is remarkably solar-like with only ¹³C, ¹⁴N, and ²²Ne isotopes showing significant abundance differences. This degree of similarity is not well explained by present specific models for the cosmic-ray origin and is discussed further in this paper.

Subject headings: cosmic rays — ISM: abundances — Sun: abundances

1. INTRODUCTION

Recent studies of the mass composition of $Z = 6$ –16 cosmic-ray nuclei using the *Voyager* (Webber et al. 1996a, 1996b) as well as the *Ulysses* (Connell & Simpson 1993a, 1993b) spacecraft have clearly identified only a few cases where the mass composition at the cosmic-ray source is different than the solar abundance. These are the isotopes ¹⁴N and ²²Ne that were shown much earlier, in fact, to have nonsolar abundances (see, e.g., Krombel & Wiedenbeck 1988; Wiedenbeck & Greiner 1981). The low ¹³C/¹²C ratio in the cosmic-ray source found by *Voyager* could be evidence for an enrichment of ¹²C in these sources rather than a depletion of ¹³C. Several isotopes originally thought to have an enhanced abundance in the cosmic-ray source such as ²⁵Mg, ²⁶Mg and ²⁹Si, ³⁰Si have been shown to have an essentially solar abundance to within 15% or less (Webber et al. 1996a). These limits place severe restrictions on models that have been proposed to explain the compositional differences between the cosmic-ray source abundances and solar abundances. This makes it especially important, in terms of understanding the origin of cosmic rays and the related nucleosynthesis, to study the mass composition of cosmic-ray elements near the Fe peak where other types of nucleosynthetic processes play a role. The Fe isotopes ⁵⁴Fe and ⁵⁸Fe are particularly sensitive (1) to conditions at the source and (2) to any differences in the standard picture for the origin of the solar system Fe abundances through the production of unstable Ni isotopes

in neutron-rich supernova environments. In addition, there are the isotopes ⁴⁰Ca, ⁵²Cr, and ⁵⁵Mn that owe their abundances to both alpha-particle burning and characteristics of the Fe-peak nucleosynthesis.

Various radioactive isotopes in this iron-group region also provide information about the timescales and densities related to the cosmic-ray propagation in the Galaxy. These include ⁵⁴Mn, whose half-life is uncertain but is believed to be $\sim 10^6$ yr. Also of interest are the so-called electron capture isotopes, ⁵⁵Fe, ⁵¹Cr, and ⁴⁹V particularly, whose decay by electron capture depends on their energy and the density of the medium being traversed and so provides information on the time of acceleration and the amount of reacceleration of the cosmic rays. Previous measurements of the overall mass composition of Fe-group nuclei have mainly focused on the measurements made by the cosmic-ray detector on the *ISEE 3* spacecraft (Leske 1993) but also include new measurements of Mn and Fe nuclei made by the high-resolution instrument on *Ulysses* (Connell & Simpson 1996).

In this paper we report on the mass composition of elements from Ca to Fe using the cosmic-ray telescopes on the *Voyager* spacecraft. A preliminary report of this data has been given by Lukasiak et al. (1995). The *Voyager* telescopes have mass resolution comparable to the previously reported *ISEE 3* data (Leske 1993) but have 2–4 times the statistics because of the long timescale of the *Voyager* mission. For many of the isotopes in question, the interpretation of the

data in terms of the cosmic-ray source composition is still statistically limited, however.

2. OBSERVATIONS AND DATA ANALYSIS

The data from the High Energy Telescope (HET) of the cosmic-ray experiment on both the *Voyager 1* and 2 spacecraft from 1977 to 1996 have been used in this analysis. This telescope (Fig. 1) has been extensively described previously (Stone et al. 1977), and the charge and mass analysis of the telescope events closely follow that described by Lukasiak et al. (1994a). The first step in the analysis of the experimental data is the removal of background events, which is accomplished by using two independent dE/dx versus E analyses to reject events that are not consistent. Using an energy-loss program, we calculated the theoretical tracks in dE/dx versus E space for each charge. These tracks are fitted to the data for the elements $Z = 20-28$ in this analysis. For every event we have determined a charge value from the position of the event with respect to the closest charge track, as described by Ferrando et al. (1991). In Figure 2 we show a scatter plot of charge consistency versus charge for the selected events with $Z = 20-28$. The overall charge resolution for these elements is ~ 0.09 charge units.

In the next stage of data analysis, we determined for each event two mass values A_1 and A_2 corresponding to the analysis of B_1 versus ΣC and B_2 versus ΣC pulse-height data, where $\Sigma C = C_2 + C_3 + C_4$ (Fig. 1). In this case, for every element we generated theoretical mass lines corresponding to the different isotopes. A mass value was then determined for every event from the position of the event with respect to the closest mass track. These simulation tracks were then further adjusted slightly to fit the distribution of events corresponding to different isotopes and to optimize the mass resolution for the key isotopes of each

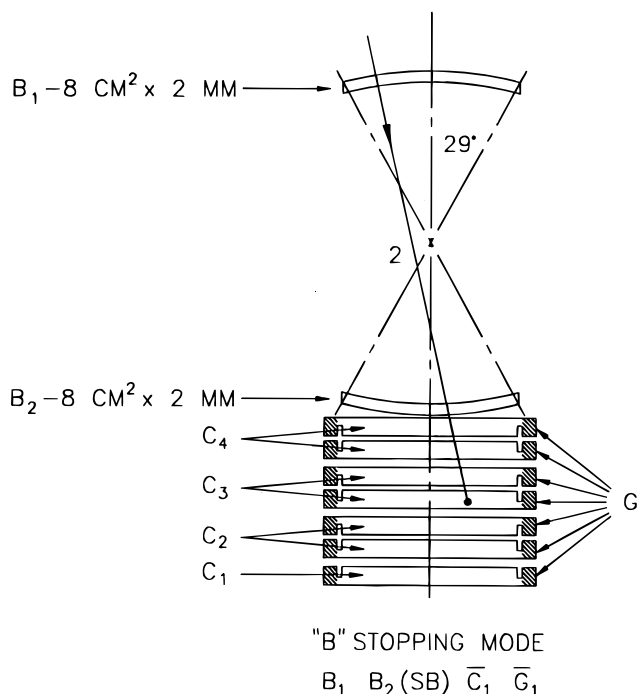


FIG. 1.—Outline drawing of the B-stopping telescope of the *Voyager* HET detector system.

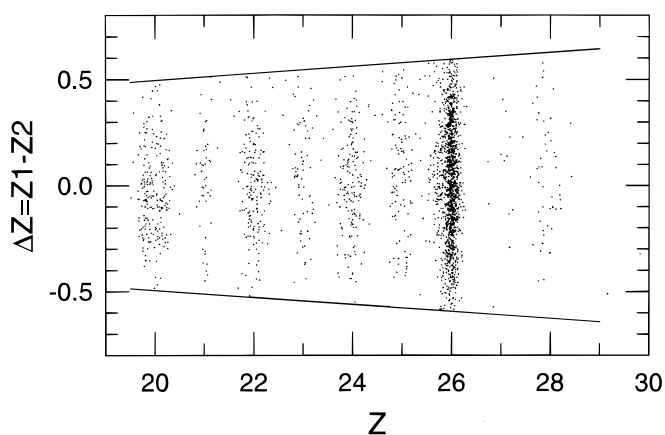


FIG. 2.—Scatter plot of charge consistency vs. charge for $Z = 20-28$ nuclei events within the 3σ (solid lines) consistency criterion.

charge such as ^{40}Ca , ^{45}Sc , and ^{56}Fe . The HET telescope has three dead layers between the C counters, and events from the dead layers have mass values that are not as well resolved. To improve the mass resolution, we removed all events that stopped in the dead layers. This decreased the number of events by $\sim 20\%$.

Figure 3 shows the mass histograms for the elements Ca through Fe in the combined *Voyager 1* and 2 spacecraft measurements from 1977 to 1996. The solid lines in Figure 3 correspond to a fit of a multi-Gaussian function to the isotope distribution for each charge. These mass functions are spaced at exactly 1.0 AMU intervals and have resolutions ranging from 0.40 AMU for ^{40}Ca to 0.60 AMU for ^{56}Fe . Using data from our previous analysis of $Z = 6-16$ nuclei (Webber et al. 1996a, 1996b), we show (Table 1 and Fig. 4) the mass resolution as a function of charge for the *Voyager* HET telescopes. The slow degradation of mass resolution with Z is mainly because of the path length variations of the trajectories through the telescope that remain constant with Z , whereas the mass separation itself is $\sim A^{-1}$.

The event breakdown and charge ratios for the different charges are given in Table 2. The charge ratios were cor-

TABLE 1
MASS RESOLUTION AS A FUNCTION
OF CHARGE

Charge	Mass Resolution σ (AMU)
Be	0.185
B	0.195
C	0.205
O	0.225
Ne	0.255
Mg	0.310
Al	0.350
Si	0.360
S	0.400
Ca	0.400
Sc	0.430
Ti	(0.470)
V	(0.510)
Cr	(0.545)
Mn	(0.575)
Fe	0.600

NOTE.—Errors typically ± 0.01 ; numbers in parentheses were interpolated.

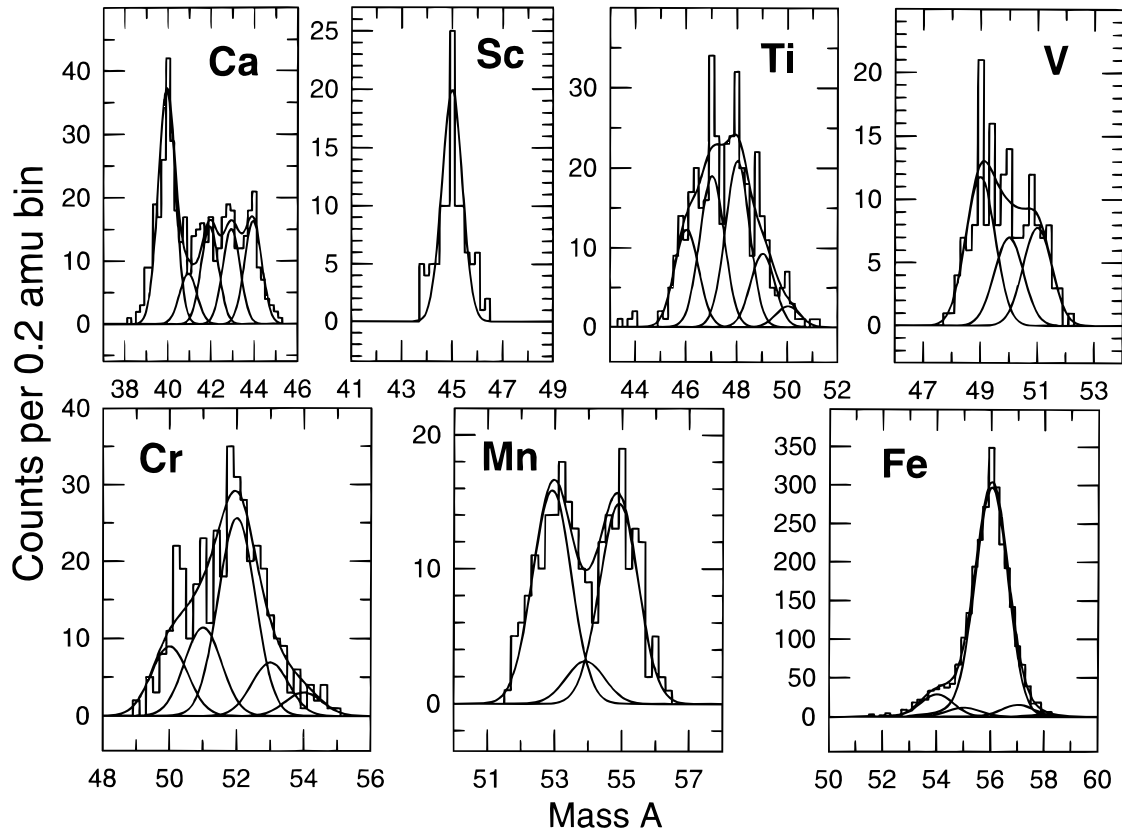


FIG. 3.—Mass histograms for the elements Ca through Fe showing fitted Gaussian functions

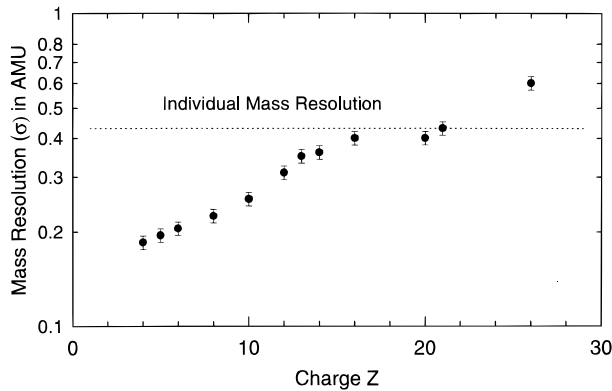


FIG. 4.—Measured mass resolution vs. charge for *Voyager* HET-B telescope events. The dotted line indicates the mass resolution necessary to just separate (produce a dip in the pulse-height distribution) two adjacent isotopes of equal abundance.

rected for the slightly different energy intervals for each charge, which resulted in differences in the widths of the energy intervals and also differences because of the spectra of the particles, assumed here to have a spectral index of 0.50 in this energy range. These effects introduced changes less than 6% in any of the charge ratios.

The errors on the measured charge ratios are dominated in some cases by the statistical errors on the number of events, e.g., ^{40}Ca , ^{53}Mn , ^{55}Mn , and ^{56}Fe , but in most cases by the included fitting errors.

The results of this 18 year study correspond to an average level of solar modulation $\phi = 480$ MV with a range ~ 220 – 1000 MV at the *Voyager* spacecraft. These modulation levels were estimated on a yearly basis using the He spectrum measured at V2 for that year and the modulation model described by Ferrando et al. (1991). The resulting

TABLE 2
COSMIC-RAY RELATIVE ELEMENTAL RATIOS

Element	Number of Events	Energy Range (MeV nucleon ⁻¹)	Measured Ratio (%)	Propagated Solar-like Abundances
Ca/Fe	576	96–260	20.99 ± 0.94	21.63
Sc/Fe	129	98–262	4.61 ± 0.41	4.31
Ti/Fe	481	100–270	16.53 ± 0.80	15.55
V/Fe	202	102–276	6.49 ± 0.47	7.15
Cr/Fe	483	105–284	15.06 ± 0.77	14.38
Mn/Fe	296	107–290	8.71 ± 0.53	8.18
Fe	3482	110–298	1.0	...
(Sc+Ti+V)/Fe	812	98–276	27.63 ± 1.08	27.01

values of ϕ for each year are shown in Figure 4 of Webber et al. (1996a). The overall average modulation for this measurement is about equivalent to the modulation observed near Earth at sunspot minimum.

3. INTERPRETATION OF RESULTS

The interpretation of these experimental results requires a model for the propagation of cosmic rays in the Galaxy. As a point of reference for earlier calculations, we performed these calculations using a standard leaky box model with a simple exponential distribution of path lengths through the interstellar material. The most essential components of this model are (1) the source composition, (2) the source spectral shape, (3) the composition of the interstellar medium (ISM), (4) the fragmentation cross sections, (5) the interstellar path lengths as a function of energy, and (6) the effects of solar modulation.

For the source composition, we took the solar system abundances (all solar source abundances are from Anders & Ebihara 1982). The source spectral shape was taken to be a power law in rigidity with an index of -2.36 . We assumed that the ISM is 90% H and 10% He by number with an ionized fraction of 30% (Soutoul, Ferrando, & Webber 1990). This ionized fraction increases the energy loss by ionization significantly over that for a neutral medium. For the interstellar fragmentation we used the measured and parametric cross sections in hydrogen given by Webber, Kish, & Schrier (1990a, 1990b, 1990c) and the helium cross sections from Ferrando et al. (1988). These helium cross sections result in less production from helium than earlier estimates, thus necessitating overall a slightly larger interstellar path length for the same total secondary production as compared with the values of Garcia-Munoz et al. (1987), for example.

For the interstellar path length we took $\lambda_{\text{esc}} = 40.6 \beta R^{-0.70}$ for rigidities $R > 3.3$ GV and $17.6\beta \text{ g cm}^{-2}$ for $R < 3.3$ GV, which provide a best fit to the $(Z = 21-23)/\text{Fe}$ ratio measured at both low and high energies (Fig. 5). For solar modulation effects we have considered values of ϕ ranging from 400 to 600 MV in order to determine the

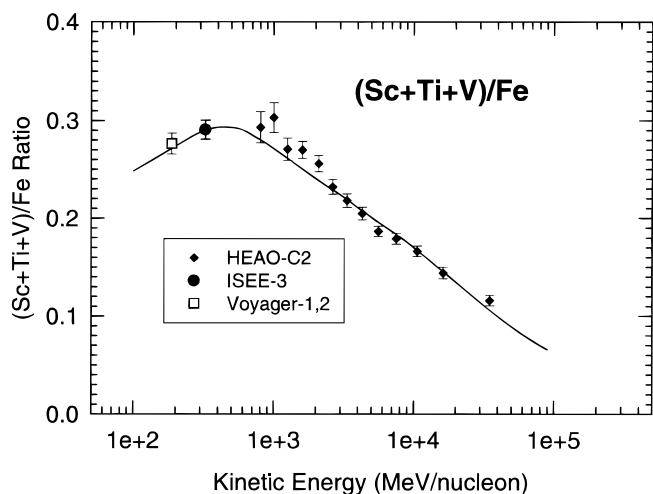


FIG. 5.—Measured $Z = (21-23)/\text{Fe}$ ratio used to determine interstellar path length for Ca through Fe nuclei. Data include this experiment and Leske (1993) (*ISEE 3*) at low energies and Engelmann et al. (1990) (*HEAO 3*) at higher energies. The solid line represents calculations for the interstellar path length $\lambda_{\text{esc}} = 40.6\beta R^{-0.70}$ for rigidities $R > 3.3$ GV and $= 17.6\beta \text{ g cm}^{-2}$ for $R < 3.3$ GV and 500 MV modulation level.

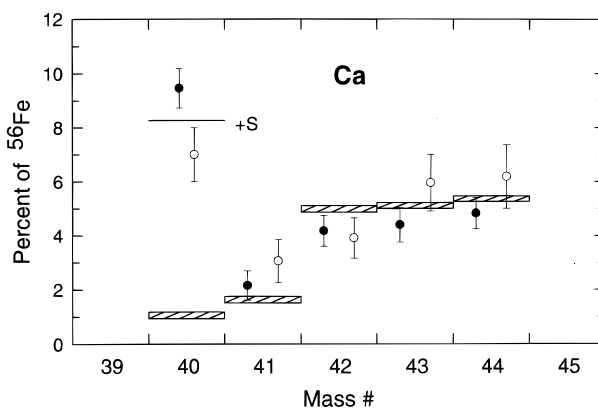


FIG. 6.—Calculated and measured abundances of Ca isotopes relative to ^{56}Fe . Filled circles: our data; open circles, Leske & Wiedenbeck (1993). The solid curves on the plot show the results of a propagation calculation, secondary contribution plus additional (ZS) solar-like source composition. The hatched boxes represent only secondary contribution.

uncertainty in the calculations as a result of uncertainties in solar modulation effects.

A comparison between our new results on the Ca through Fe elements and the propagation calculations is shown in Tables 3 and 4 and in Figures 6–8. Previous results on these elements from the *ISEE* experiment (Leske 1993) and *Ulysses* results for Fe (Connell & Simpson 1997) are shown along with our data in Figures 6–8. We wish to point out, however, that the statistics of the new results are up to a factor ~ 4 better than the earlier results (Leske 1993) with approximately the same mass resolution. The assignment of measurement errors for our new results has already been discussed. For the errors on the secondary contribution, which includes both Galactic propagation and solar modulation uncertainties, we have assumed that the overall error caused by cross section uncertainties is $\pm 5\%$ for the measured cross sections and $\pm 15\%$ for those obtained from the formula as per our earlier calculation (Lukasiak et al. 1994a, 1994b). For the uncertainty in the interstellar path length, we took the value of $17.6\beta \pm 10\%$, below 3.3 GV. And, finally, for the modulation, we took an uncertainty of ± 50 MV. The total error for the secondary calculation was

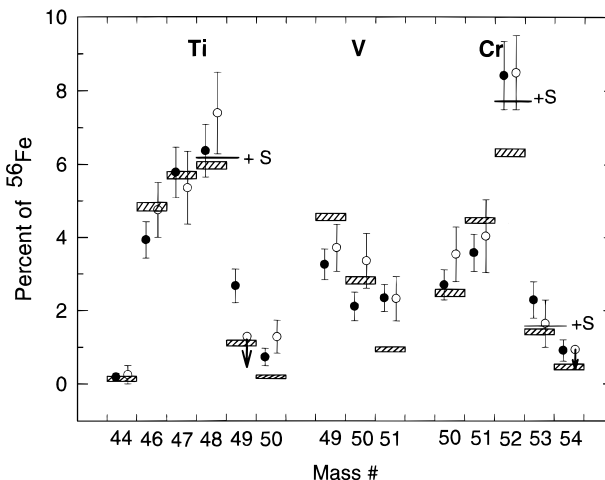


FIG. 7.—Calculated and measured abundances of Ti, V, and Cr isotopes relative to ^{56}Fe . Filled circles: our data; open circles, Leske (1993). The solid lines and hatched boxes are as in Fig. 6.

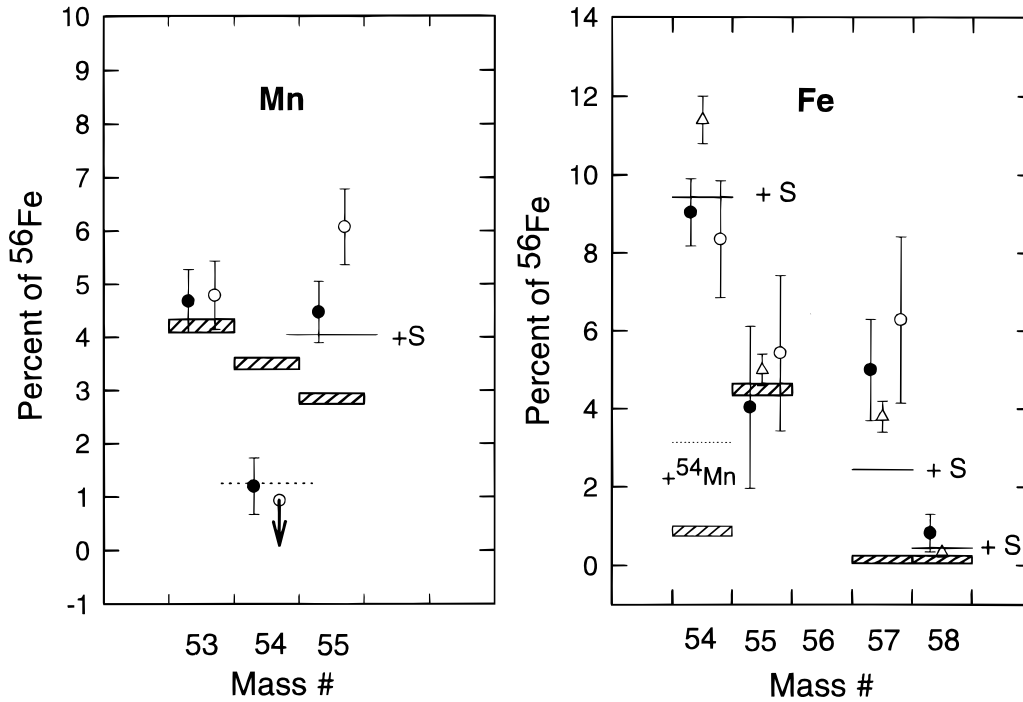


FIG. 8.—Calculated and measured abundances of Mn isotopes relative to ^{56}Fe . Data symbols are the same as in Fig. 7 plus open triangles from Connell & Simpson (1996). The dotted line shows the result of a propagation calculations when ^{54}Mn β decays with a half-life equal to 1.0×10^6 yr. The solid lines and hatched boxes are as in Fig. 6.

then obtained by adding the above errors in quadrature (see below for an alternate estimate of the propagational errors using the tracer technique [Stone & Wiedenbeck 1979] with $Z = 21\text{--}23$ nuclei, which actually leads to a significantly smaller uncertainty than that estimated above).

We will now discuss the mass distribution obtained as a function of charge.

Calcium.—Calcium is dominated by the isotope ^{40}Ca , which constitutes 0.38 ± 0.02 of all Ca. This fraction, taken with the total measured Ca/Fe charge ratio of 0.210 ± 0.009 and the measured ^{56}Fe fraction of 0.841 of Fe, leads to a $^{40}\text{Ca}/^{56}\text{Fe}$ ratio of 0.084 ± 0.007 at the source as compared with a solar abundance ratio of 0.072 . Thus the $^{40}\text{Ca}/^{56}\text{Fe}$ ratio we deduce at the source is 1.16 ± 0.10 times the solar

TABLE 3
COSMIC-RAY ISOTOPIC COMPOSITION

Element	Number of Events	Energy Range (MeV nucleon $^{-1}$)	Measured Ratio (%)	Propagated Solar-like Abundances
$^{40}\text{Ca}/\text{Ca}$	177,467	96–260	37.9 ± 2.2	33.3
$^{41}\text{Ca}/\text{Ca}$	40	96–260	8.6 ± 2.1	6.3
$^{42}\text{Ca}/\text{Ca}$	78	96–260	16.7 ± 2.1	19.4
$^{43}\text{Ca}/\text{Ca}$	82	96–260	17.6 ± 2.4	20.2
$^{44}\text{Ca}/\text{Ca}$	90	96–260	19.3 ± 2.1	20.8
$^{44}\text{Ti}/\text{Ti}$	4,386	99–268	0.95 ± 0.48	0.76
$^{46}\text{Ti}/\text{Ti}$	79	99–268	20.0 ± 2.3	26.6
$^{47}\text{Ti}/\text{Ti}$	112	99–268	29.4 ± 3.1	31.4
$^{48}\text{Ti}/\text{Ti}$	121	99–268	32.4 ± 3.2	34.1
$^{49}\text{Ti}/\text{Ti}$	54	99–268	13.6 ± 2.2	6.1
$^{50}\text{Ti}/\text{Ti}$	16	99–268	3.7 ± 1.2	1.1
$^{49}\text{V}/\text{V}$	70,170	101–277	42.3 ± 4.4	54.5
$^{50}\text{V}/\text{V}$	48	101–277	27.4 ± 4.6	33.8
$^{51}\text{V}/\text{V}$	52	101–277	30.3 ± 4.2	11.7
$^{50}\text{Cr}/\text{Cr}$	63,387	104–283	15.1 ± 2.1	14.8
$^{51}\text{Cr}/\text{Cr}$	102	104–283	20.0 ± 2.6	26.8
$^{52}\text{Cr}/\text{Cr}$	153	104–283	47.0 ± 4.4	46.0
$^{53}\text{Cr}/\text{Cr}$	51	104–283	12.8 ± 2.7	9.4
$^{54}\text{Cr}/\text{Cr}$	18	104–283	5.1 ± 1.6	2.7
$^{53}\text{Mn}/\text{Mn}$	102,238	106–290	45.2 ± 4.9	44.3
$^{54}\text{Mn}/\text{Mn}$	32	106–290	11.6 ± 5.1	13.1
$^{55}\text{Mn}/\text{Mn}$	104	106–290	43.2 ± 4.8	42.6
$^{54}\text{Fe}/\text{Fe}$	258,2692	109–298	7.6 ± 0.7	8.1
$^{55}\text{Fe}/\text{Fe}$	89	109–298	< 5.1	3.8
$^{56}\text{Fe}/\text{Fe}$	2197	109–298	84.1 ± 2.1	85.6
$^{57}\text{Fe}/\text{Fe}$	129	109–298	< 5.3	2.1
$^{58}\text{Fe}/\text{Fe}$	19	109–298	0.7 ± 0.4	0.4

TABLE 4
COSMIC-RAY ISOTOPIC RATIOS RELATIVE TO ^{56}Fe

Element	Measured Ratio (%)	Propagated Solar-like Abundances	(Expected – Propagated)/ Δ Expected
$^{40}\text{Ca}/^{56}\text{Fe}$	9.46 ± 0.73	8.27	+1.62 σ
$^{41}\text{Ca}/^{56}\text{Fe}$	2.15 ± 0.54	1.60	+1.02 σ
$^{42}\text{Ca}/^{56}\text{Fe}$	4.17 ± 0.57	4.96	-1.40 σ
$^{43}\text{Ca}/^{56}\text{Fe}$	4.39 ± 0.64	5.15	-1.18 σ
$^{44}\text{Ca}/^{56}\text{Fe}$	4.82 ± 0.58	5.29	-0.82 σ
$^{44}\text{Ti}/^{56}\text{Fe}$	0.19 ± 0.10	0.14	+0.5 σ
$^{46}\text{Ti}/^{56}\text{Fe}$	3.93 ± 0.50	4.84	-1.8 σ
$^{47}\text{Ti}/^{56}\text{Fe}$	5.78 ± 0.69	5.70	+0.11 σ
$^{48}\text{Ti}/^{56}\text{Fe}$	6.37 ± 0.72	6.18	+0.26 σ
$^{49}\text{Ti}/^{56}\text{Fe}$	2.67 ± 0.46	1.11	+3.4 σ
$^{50}\text{Ti}/^{56}\text{Fe}$	0.73 ± 0.24	0.19	+2.2 σ
$^{49}\text{V}/^{56}\text{Fe}$	3.26 ± 0.42	4.56	-3.1 σ
$^{50}\text{V}/^{56}\text{Fe}$	2.11 ± 0.39	2.82	-1.8 σ
$^{51}\text{V}/^{56}\text{Fe}$	2.34 ± 0.37	0.98	+3.7 σ
$^{50}\text{Cr}/^{56}\text{Fe}$	2.70 ± 0.41	2.48	+0.55 σ
$^{51}\text{Cr}/^{56}\text{Fe}$	3.58 ± 0.51	4.47	-1.75 σ
$^{52}\text{Cr}/^{56}\text{Fe}$	8.42 ± 0.92	7.73	0.74 σ
$^{53}\text{Cr}/^{56}\text{Fe}$	2.29 ± 0.50	1.58	+1.42 σ
$^{54}\text{Cr}/^{56}\text{Fe}$	0.91 ± 0.29	0.46	+1.56 σ
$^{53}\text{Mn}/^{56}\text{Fe}$	4.68 ± 0.59	4.21	+0.8 σ
$^{54}\text{Mn}/^{56}\text{Fe}$	1.20 ± 0.53	1.25	-0.09 σ
$^{55}\text{Mn}/^{56}\text{Fe}$	4.47 ± 0.58	4.04	+0.75 σ
$^{54}\text{Fe}/^{56}\text{Fe}$	9.04 ± 0.86	9.44	-0.51 σ
$^{55}\text{Fe}/^{56}\text{Fe}$	< 6.0	4.49	...
$^{57}\text{Fe}/^{56}\text{Fe}$	< 6.3	2.44	...
$^{58}\text{Fe}/^{56}\text{Fe}$	0.83 ± 0.48	0.44	+0.8 σ

ratio: slightly enhanced but not significantly so. This new source ratio is consistent with earlier measurements, as summarized in Figure 6.

The heavier isotopes ^{42}Ca , ^{43}Ca , and ^{44}Ca are observed to have nearly equal abundances and are in agreement with the calculations for purely secondary production as shown in Tables 3 and 4 and in Figure 6.

Scandium.—The single isotope ^{45}Sc gives a ratio Sc/Fe of 0.046 ± 0.004 , which is almost identical with the predicted purely secondary ratio of 0.043. This single isotope exhibits a mass resolution σ of ~ 0.42 AMU—almost the same as the value of 0.40 AMU observed for ^{40}Ca .

Titanium.—This charge shows a complex distribution of isotopes, all dominated by secondary production in the interstellar medium. There is good agreement between the observed and predicted isotope fractions with the possible exception of ^{49}Ti (see Tables 3 and 4 and Fig. 7), which is a decay product of the electron capture isotope ^{49}V . All three K-electron capture isotopes ^{49}V , ^{51}Cr , and ^{55}Fe will be discussed in a separate paper (Soutoul et al. 1997).

Vanadium.—This charge has three isotopes, all completely dominated by secondary production. Here ^{49}V shows a lower mass fraction than predicted from purely secondary production, and ^{51}V shows a considerably larger mass fraction than predicted (Tables 3 and 4 and Fig. 7). ^{49}V is an electron capture isotope, and ^{51}V is the decay product of the electron capture isotope ^{51}Cr .

Z = 21–23 nuclei.—Because they contain no significant source fraction, these charges provide an excellent tracer of the total amount of secondary interstellar production from nuclear interactions in hydrogen and helium and also of solar modulation effects, as well as uncertainties in these two effects in the same way that boron does for lower Z nuclei and ^{21}Ne (or Fl) does for intermediate Z nuclei (Stone & Wiedenbeck 1979). The observed $(Z = 21\text{--}23)/\text{Fe}$ ratio at 205 MeV nucleon $^{-1}$ is 0.276 ± 0.011 as compared

with the calculated ratio of 0.27 (Table 2 and Fig. 5). So this agreement between these measured and calculated tracer charges indicates that any systematic uncertainties in either the propagation calculation including cross sections or modulation effects, for the Ca through Fe isotopes considered here, must be known to be $\pm 4\%$ or less, which is the uncertainty in the difference between the measured and calculated $(Z = 21\text{--}23)/\text{Fe}$ ratios. This uncertainty is less than the total sum of the formal uncertainties discussed above, which is typically $\sim 10\%$ of the total secondary production.

Chromium.—This charge also shows a complex distribution of isotopes, but it is clearly dominated by ^{52}Cr . Only ^{52}Cr is expected to have a significant source abundance. The measured Cr isotopes show some differences with the predicted ones (see Tables 3 and 4 and Fig. 7). The measured ^{51}Cr abundance is ~ 2 σ low, and ^{54}Cr is somewhat high. Again, both of these isotopes are K-capture isotopes. For ^{52}Cr the source abundance relative to ^{56}Fe that we deduce is 0.020 ± 0.009 or 1.51 ± 0.68 times the solar fraction of 0.0136 (Tables 3 and 4 and Fig. 7).

Manganese.—Manganese is dominated by the isotopes ^{53}Mn and ^{55}Mn , with only a weak presence of the radioactive decay isotope ^{54}Mn . The observed ^{53}Mn and ^{55}Mn fractions are consistent with the secondary calculations assuming a solar abundance of ^{55}Mn at the cosmic-ray source (see Tables 3 and 4 and Fig. 8). The deduced $^{55}\text{Mn}/^{56}\text{Fe}$ ratio at the source is 0.016 ± 0.006 or 1.35 ± 0.48 times the solar ratio of 0.0121 (assuming no decay by K-electron capture of ^{55}Fe into ^{55}Mn).

The measured ^{54}Mn abundance fraction is 0.34 ± 0.15 of that expected if no decay has occurred. This surviving fraction would imply a ^{54}Mn half-life of $(1.0 \pm 0.6) \times 10^6$ yr, assuming the same interstellar density ($\rho = 0.3$ atoms cm^{-3}) as that used for the lower Z radioactive nuclei ^{10}Be and ^{26}Al with comparable half-lives. The amount of decaying ^{54}Mn amounts to $(0.0235 \pm 0.0053) \times ^{56}\text{Fe}$, a significant

fraction of which will enhance the ^{54}Fe abundance, thus providing a check on the fraction of ^{54}Mn that has decayed. (The above calculation assumes no K-capture decay of ^{54}Mn to ^{54}Cr ; if this decay has occurred, the deduced lifetime of ^{54}Mn for β decay will be longer, and the source abundance of ^{54}Fe will change by $<10\%$. This will be discussed in a forthcoming paper, Soutoul et al. 1997).

Iron.—Iron is completely dominated by ^{56}Fe in our data—this isotope constitutes 0.84 ± 0.02 of all iron. Our mass resolution of 0.60 AMU does not allow significant values to be obtained for the isotope fractions of the interesting isotopes ^{55}Fe and ^{57}Fe , which are separated from ^{56}Fe by ± 1 AMU. Both of these isotopes would be expected to be present at the few percent level if they had solar abundances. However, for the isotopes ^{54}Fe and ^{58}Fe , separated by ± 2 AMU, the mass resolution of 0.60 AMU is equivalent to 0.30 AMU for isotopes separated by ± 1 AMU. We have seen that for ~ 0.30 AMU mass resolution, the isotopes of Ne and Mg can be well resolved (Webber et al. 1996a) so one would expect to obtain useful limits on the ^{54}Fe and ^{58}Fe mass fractions from this measurement. For the analysis of Fe isotopes, we have assumed a tail on the low-mass side of the Fe isotope distributions. This tail contains $2.0\% \pm 0.6\%$ of all ^{56}Fe events and is based on the tail observed for ^{28}Si (and used in the correction of ^{26}Al – ^{27}Al distribution by Lukasiak et al. 1994b). We believe this tail, which is present in all distributions regardless of resolution, is a geometrical effect and therefore is independent of Z . This tail reduced the $^{54}\text{Fe}/^{56}\text{Fe}$ ratio by $\sim 20\%$.

For ^{54}Fe , the measured $^{54}\text{Fe}/^{56}\text{Fe}$ ratio of 0.090 ± 0.009 (using the tail correction and based on 260 events) compares with a calculated ratio of 0.094. This calculated ratio includes a solar source component of $0.063 \times ^{56}\text{Fe}$, the decay of $^{54}\text{Mn} = 0.023 \times ^{56}\text{Fe}$, and direct secondary production (see Fig. 8). The deduced source ratio for $^{54}\text{Fe}/^{56}\text{Fe}$ after subtracting the ^{54}Mn decay and secondary production from the measured ratio is thus 0.0585 ± 0.0086 or 0.93 ± 0.14 times the solar ratio of 0.063, which is consistent with the solar abundance.

For the $^{58}\text{Fe}/^{56}\text{Fe}$ ratio, our measured value of 0.008 ± 0.005 is dominated by fitting uncertainties. The predicted ratio assuming a solar source ratio is 0.0044, so our value is somewhat higher than but consistent with the solar ratio.

4. SUMMARY AND CONCLUSIONS

We have measured the isotopic composition of cosmic-ray Ca through Fe nuclei with improved statistical accuracy using the HET telescopes on the *Voyager* spacecraft. This is achieved as a result of the 18 year data base from the mission. The mass resolution, σ , ranges from 0.40 to 0.60 AMU—about the same as that obtained from the cosmic-ray detector on the *ISEE* spacecraft, the best previous measurement involving all of these charges. Most of the isotopes of these charges are dominated by interstellar secondary production from cosmic rays traversing the interstellar medium. For these isotopes, our measured isotopic ratios with respect to ^{56}Fe are generally consistent to within $\pm 10\%$ with those expected from purely secondary production (except for the K-electron capture isotopes).

We observe a $^{54}\text{Mn}/^{56}\text{Fe}$ ratio ~ 0.34 of that expected from interstellar propagation if no decay has occurred. This survival fraction translates into a ^{54}Mn decay lifetime of $(1.0 \pm 0.6) \times 10^6$ yr assuming this isotope has the same pro-

pagation history as the lower Z radioactive nuclei ^{10}B and ^{26}Al and not allowing for any additional ^{54}Mn decay to ^{54}Cr by K-electron capture.

For five isotopes, ^{40}Ca , ^{52}Cr , ^{55}Mn , ^{54}Fe , and ^{58}Fe , we can determine the source composition to an improved accuracy over previous measurements (see, however, the *Ulysses* measurements of ^{54}Fe and ^{58}Fe by Connell & Simpson 1996). None of these isotopic ratios with respect to ^{56}Fe measured by *Voyager* show any significant differences with solar composition to accuracies ranging from $\sim 20\%$ to a factor of ~ 2 for ^{58}Fe . This observation—when coupled with the fact that in the $Z = 6$ – 16 charge range, only ^{14}N and ^{22}Ne (and possibly ^{13}C) out of 10 isotopes whose source composition can be reasonably determined using the *Voyager* data show any significant differences from solar (Webber et al. 1996a, 1996b) and also that new *Voyager* results on Co and Ni isotopes (Lukasiak et al. 1996) show a normal solar composition as well for all five of these isotopes that can be measured, in agreement with the latest results on Fe through Ni nuclei from the high-resolution instrument on *Ulysses* (Connell & Simpson 1997)—suggests that the cosmic-ray source isotopic composition is remarkably solar-like, with few very distinctive differences.

The complete list of cosmic-ray source–solar isotope ratios measured by *Voyager* and other recent experiments is given in Table 5. This should be compared with the summary given by Mewaldt (1989), in which, in addition to the isotopic differences observed in the *Voyager* data, the cosmic-ray source isotopic ratios of $^{18}\text{O}/^{16}\text{O}$, $^{25}\text{Mg}/^{24}\text{Mg}$, $^{26}\text{Mg}/^{24}\text{Mg}$, $^{60}\text{Ni}/^{58}\text{Ni}$, and possibly $^{29}\text{Si}/^{28}\text{Si}$ and $^{30}\text{Si}/^{28}\text{Si}$ were all believed to be higher than the solar ratios. This suggested at that time a possible systematic difference between the cosmic-ray source and solar composition that could be related to a different nucleosynthesis history of the two samples. Two suggestions to explain the difference have been extensively discussed. One is the Wolf-Rayet model (Casse & Paul 1982) in which a fraction of the Galactic cosmic rays come from the vicinity of Wolf-Rayet stars and are enriched in ^{22}Ne and ^{25}Mg and ^{26}Mg , which are the results of helium burning in these stars.

The other model proposes that the observed excess of neutron-rich isotopes might result if cosmic rays originate in regions of the Galaxy that are metal rich compared to the solar system (Woosley & Weaver 1981). Both of these models predict an excess of neutron-rich isotopes much greater than what is now observed, as depicted by Figure 13 of Mewaldt's (1989) review.

An update of the situation in 1993–1994 may be found in the review by Ferrando (1993). At this time the first data from *Voyager* (Lukasiak et al. 1994a, 1994b) and *Ulysses* (Connell & Simpson 1993a, 1993b) were appearing, new cross section data were available (Webber et al. 1990), and the earlier excess of the neutron-rich Mg and Si isotopes was now much less pronounced.

Now with the new *Voyager* data (as summarized in Table 5) as well as new *Ulysses* data (Connell & Simpson 1997), there are only a few very distinctive abundance differences as discussed earlier. These differences still seem to point to a Wolf-Rayet contribution to the cosmic-ray sources as a result of the combination of an overabundance of ^{22}Ne (and possibly ^{12}C) and the corresponding underabundance of ^{14}N (and ^{13}C), which seems to be distinctive of the helium-burning process known to occur in these stars. Just how much of this material is actually expelled into the local

TABLE 5
COSMIC-RAY SOURCE/SOLAR ISOTOPE RATIOS

Ratio	<i>Voyager</i> Measurements ^a	Other Recent Measurements	Prediction ^b
¹³ C/ ¹² C	0.09 ± 0.36	...	0.6 W-R
¹⁴ N/ ¹⁶ O	0.41 ± 0.04
¹⁵ N/ ¹⁶ O	2.62 ± 1.65
¹⁸ O/ ¹⁶ O	1.04 ± 0.72	...	0.7 W-R
²² Ne/ ²⁰ Ne	4.72 ± 0.43	...	3.5 W-R
²⁵ Mg/ ²⁴ Mg	1.06 ± 0.12	...	1.5 W-R
²⁶ Mg/ ²⁴ Mg	1.15 ± 0.11	...	1.5 W-R
²⁹ Si/ ²⁸ Si	0.80 ± 0.18	...	1.8 SM
³⁰ Si/ ²⁸ Si	1.03 ± 0.16	...	1.8 SM
³⁴ S/ ³² S	1.07 ± 0.67	1.41 ± 0.66 ^c	1.8 SM
⁴⁰ Ca/ ⁵⁶ Fe	1.16 ± 0.10
⁵² Cr/ ⁵⁶ Fe	1.51 ± 0.68
⁵⁵ Mn/ ⁵⁶ Fe	1.35 ± 0.48
⁵⁴ Fe/ ⁵⁶ Fe	0.93 ± 0.14	1.50 ± 0.10 ^d	1.5 SM
⁵⁸ Fe/ ⁵⁶ Fe	1.48 ± 0.75	0.50 ± 0.35 ^d	1.8 SM
⁵⁹ Co/ ⁵⁶ Fe	1.23 ± 0.40
⁵⁸ Ni/ ⁵⁶ Fe	0.96 ± 0.15	0.95 ± 0.11 ^d	...
⁶⁰ Ni/ ⁵⁶ Fe	0.99 ± 0.24	1.23 ± 0.18 ^d	...
⁶² Ni/ ⁵⁶ Fe	0.76 ± 0.40	0.90 ± 0.35 ^d	...

NOTE.—(W-R = Wolf-Rayet model, SM = supermetallicity model)

^a Webber et al. 1996a, 1996b plus this measurement.

^b Mewaldt 1989.

^c Thayer 1997.

^d Connell & Simpson 1997.

interstellar medium by the high-velocity winds from these stars (see, e.g., Prantzos et al. 1986) remains uncertain, however, and may be best determined by the observed cosmic-ray composition itself.

The authors wish to thank the *Voyager* Project Office at JPL for their support through contract 959213 at the University of Maryland and contract 959160 at New Mexico State University.

REFERENCES

- Anders, E., & Ebihara, M. 1982, *Geochim. Cosmochim. Acta*, 4b, 2363
 Casse, M., & Paul, J. A. 1982, *ApJ*, 258, 860
 Connell, J. J., & Simpson, J. A. 1993a, *Proc. 23d Int. Cosmic-Ray Conf. (Calgary)*, 1, 547
 ———, 1993b, *Proc. 23d Int. Cosmic-Ray Conf. (Calgary)*, 1, 559
 ———, 1997, *ApJ*, 475, L61
 Engelmann, J. J., et al. 1990, *A&A*, 233, 96
 Ferrando, P. 1993, *Proc. 23d ICRC Calgary, Invited, Rapporteur, and Highlight Papers*, 279
 Ferrando, P., et al. 1988, *Phys. Rev. C*, 37, 1490
 Ferrando, P., Lal, N., McDonald, F. B., & Webber, W. R. 1991, *A&A*, 247, 163
 Garcia-Munoz, M., et al. 1987, *ApJ* 64, 269
 Krombel, K. E., & Wiedenbeck, M. E. 1988, *ApJ*
 Leske, R. A. 1993, *ApJ*, 405, 567
 Leske, R. A., & Wiedenbeck, M. E. 1993, *Proc. 23d Int. Cosmic-Ray Conf. (Calgary)*, 1, 571
 Lukasiak, A., Ferrando, P., McDonald, F. B., & Webber, W. R. 1994a, *ApJ*, 426, 366
 ———, 1994b, *ApJ* 430, L69
 Lukasiak, A., McDonald, F. B., Webber, W. R., & Ferrando, P. 1995, *Proc. 24th Int. Cosmic-Ray Conf. (Rome)*, 2, 576
 Lukasiak, A., McDonald, F. B., Webber, W. R., & Ferrando, P. 1997, in *Proc. of 31st Scientific Assembly of COSPAR, Birmingham*, 19, 747
 Mewaldt, R. A. 1989, in *AIP Conf. Proc. 183, Cosmic Abundances of Matter*, ed. C. J. Waddington (New York: AIP) 124
 Prantzos, N., Doom, C., Arnould, M., & deLoore, C. 1986, *ApJ*, 304, 695
 Soutoul, A., Ferrando, P., & Webber, W. R. 1990, *Proc. 21st Int. Cosmic-Ray Conf. (Adelaide)*, 3, 337
 Soutoul, A., et al. 1997, in preparation
 Stone, E. C., et al. 1977, *Space Sci. Rev.*, 21, 355
 Stone, E. C., & Wiedenbeck, M. J. E. 1979, *ApJ*, 231, 606
 Thayer, M. R. 1997, 482, 792
 Webber, W. R., Kish, J. C., & Schrier, D. A. 1990a, *Phys. Rev. C*, 41, 520
 ———, 1990b, *Phys. Rev. C*, 41, 533
 ———, 1990c, *Phys. Rev. C*, 41, 547
 Webber, W. R., Lukasiak, A., & McDonald, F. B. 1996a, *ApJ*, 476, 766
 Webber, W. R., Lukasiak, A., McDonald, F. B., & Ferrando, P. 1996b, *ApJ* 457, 435
 Webber, W. R., Soutoul, A., Ferrando, P., & Gupta, M. 1990d, *ApJ* 348, 611
 Wiedenbeck, M. E., & Greiner, D. E. 1981, *Phys. Rev.*, 46, 682
 Woosley, S. E., & Weaver, T. A. 1981, *ApJ*, 243, 561